Supporting information

A Facile Online Multi-gear Capacitively Coupled Contactless Conductivity Detector for Automatic and Wide Range Monitoring of High Salt in HPLC

Weiwen Liu[a#], Ziqi Liang[a#], Yuanyu Wang[a], Jun Cao,[a] Qiang Zhang,[a,*] Xiaoping Liu,[a] Yuxing Wang,[c] and Chengxi Cao[a,b*1]

[a] *Department of Instrument Science and Engineering, School of Electronic Information and Electrical Engineering, Shanghai Jiao Tong University, Shanghai 200240, China*

[b] *School of Life Sciences and Biotechnology, State Key Laboratory of Microbial Metabolism, Shanghai Jiao Tong University, Shanghai 200240, China*

[c] *School of Physics and Astronomy, Shanghai Jiao Tong University, Shanghai 200240, China*

Keywords: automation; bioprocess; capacitively coupled contactless conductivity detection; electrolyte concentration; online process monitoring.

Abbreviations: M-C^{4}D, multi-gear capacitively coupled contactless conductivity detection; **RS**, relative sensitivity.

S1. The software used for monitoring conductivity via M-C^{4}D sensor

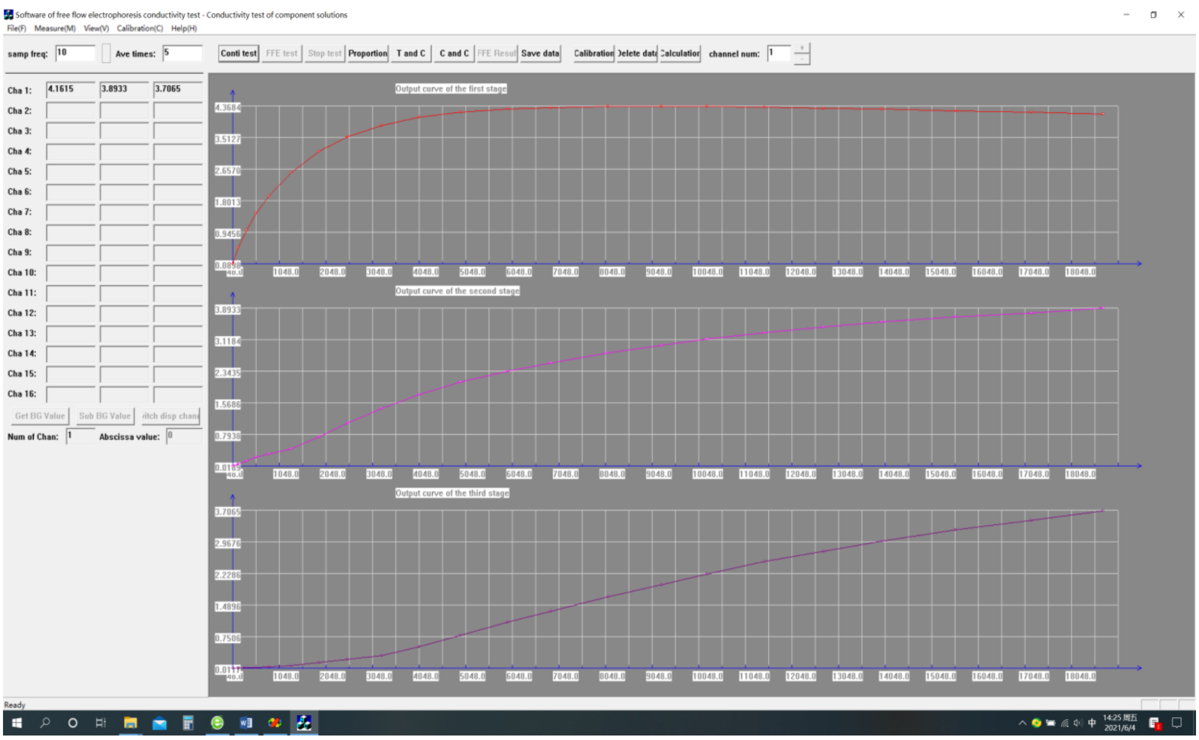

Figure S1. The screenshot of software platform.

---

1 The 1st and 2nd correspondence authors: Dr. Chengxi Cao (cxcao@sjtu.edu.cn) and Dr. Q. Zhang (billy_zq@sjtu.edu.cn).

# The first two authors have equal contribution to the work, the first gave the idea, performed the experiments, analyses and manuscript, and the second conducted model and computation, and performed the experiments and writing.

S2. The least squares polynomial fitting

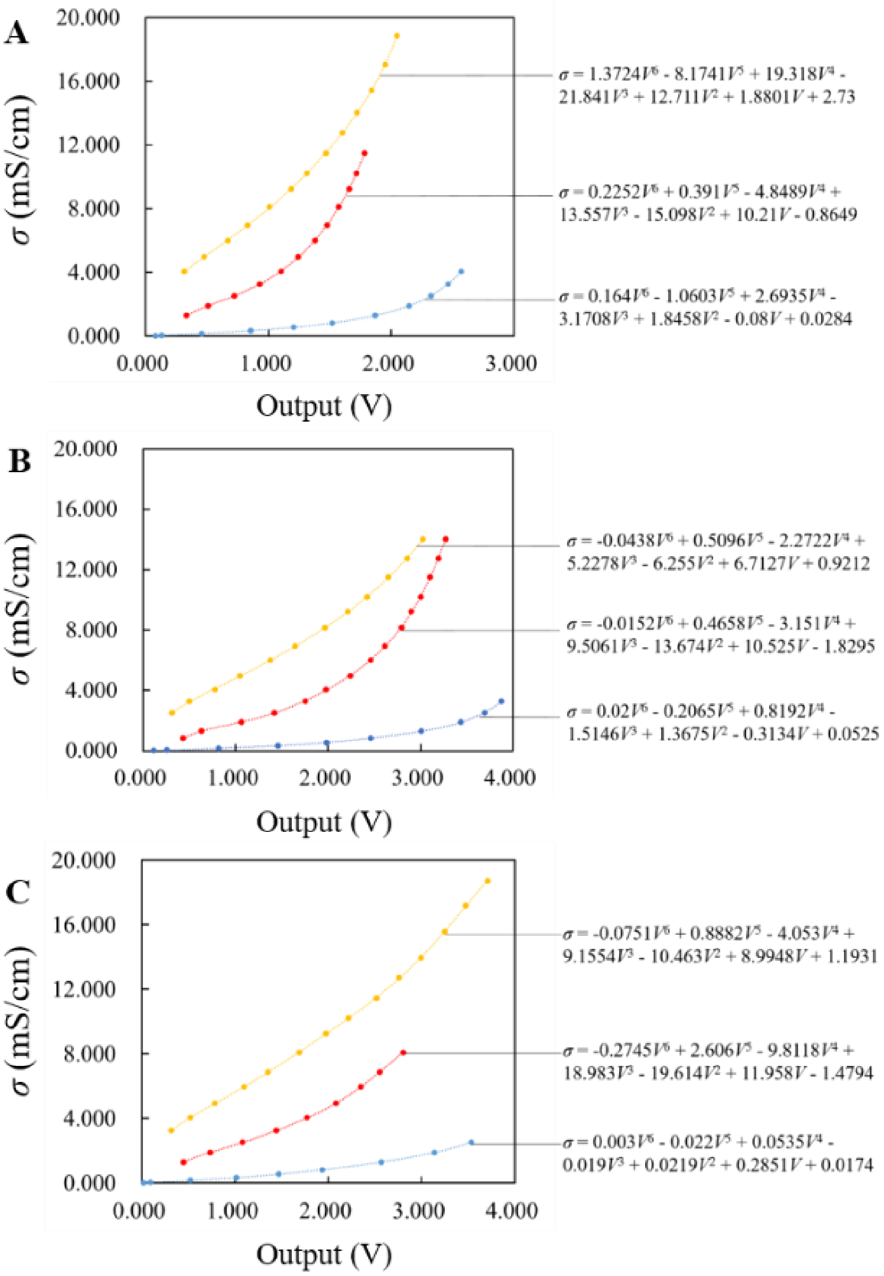

Figure S2. The least squares polynomial fitting. (**A**) r_i = 0.375 mm. (**B**) r_i = 0.5 mm. (**C**) r_i = 0.7 mm.

S3. Discussion on the method of expanding the measurement range via reducing Z_c/Z

The nonlinear output and poor sensitivity of the contactless conductivity detection sensor limit its measurement range due to the influence of coupled capacitances. In this paper, the measurement range of this type of sensor could be expanded by reducing Z_c/Z was presented. We would discuss it in detail below.

In eq. (7), (8) and (12), it can be observed that the capacitive reactance ($Z_c = 1/\omega C$) of the coupled capacitances is related to ω, r_o, r_i, l_1 and l_2, the impedance (R) of the solution is related to σ, r_i, d, l_1 and l_2, and the sensitivity of the M-C^{4}D sensor is related to σ, ω, r_o, r_i, d, l_1 and l_2. Here, we used eq. (12) as well as the above boundary conditions in Section 2.3 to draw the sensitivity characteristic curves of the M-C^{4}D sensor with different sensing section parameters and frequency (**Figure S3)** and the characteristic curves of Z_c/Z and d, r_i, l_2, f with different conductivities (**Figure S4**). **Figure S3** showed that increasing the gap (d), or the inner radius (r_i) or the electrode length (l_2) or reducing the frequency (f) was beneficial to improve the sensitivity of the contactless conductivity detection sensor at higher conductivities. **Figure S4** indicated that increasing the gap (d), or the electrode length (l_2), or the frequency (f) could reduce Z_c/Z. As for the inner radius (r_i), it could be observed from the **Figure S4B** that Z_c/Z increased firstly and then decreased with the increase of r_i, and had a maximum value when r_i was at about 0.5 mm. In addition, **Figure S4** further revealed that Z_c/Z became larger and larger with the increase of σ. Hence, we thought that a wider measurement range could be achieved via the mechanism of M-C^{4}D according to above analysis.

To verify the theory of expanding the measurement range by reducing Z_c/Z, we designed three kind of sensors with different inner radii of insulating pipe as described in Section 2.4 and calculated Z_c/Z in different gears at σ of 7 mS/cm. **Table S1** showed that the values of Z_c/Z of the first gear with inner radii of 0.375 mm, 0.5 mm and 0.7 mm were respectively 0.93, 0.94 and 0.84, the ones of the second gear were 0.7, 0.74 and 0.52, respectively, and the ones of third gear were respectively 0.47, 0.50 and 0.31. These revealed that the value of Z_c/Z of the first gear was the largest, the one of the third gear was the smallest, and the one of second gear was within the ones of the first and third gears.

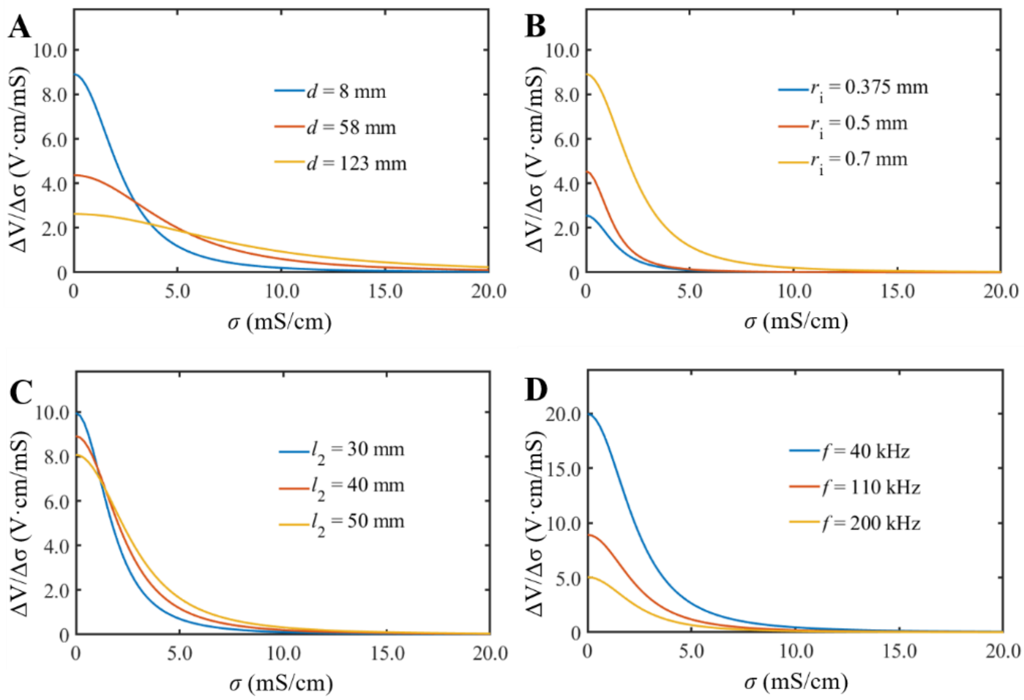

Figure S3. Sensitivity characteristic curves of the new sensor with different sensing section parameters and frequency. Digital computation parameters: $\varepsilon_0 = 8.8542\times10^{-12}$ F/m, $\varepsilon_r = 3.2$, $R_f = 1$ MΩ, $C_f = 5$ pF, $V_{pp} = 20$ V, $r_o = 0.8$ mm. (**A**) $d = 8$ mm, or 58 mm, or 123 mm, $l_1 = 40$ mm, $l_2 = 40$ mm, $r_i = 0.7$ mm and $f = 110$ kHz.

(**B**) d = 8 mm, l_1 = 40 mm, l_2 = 40 mm, r_i = 0.375 mm, or 0.5 mm, or 0.7 mm and f = 110 kHz. (**C**) d = 8 mm, l_1 = 40 mm, l_2 = 30 mm, or 40 mm, or 50 mm, r_i = 0.7 mm and f = 110 kHz. (**D**) d = 8 mm, l_1 = 40 mm, l_2 = 40 mm, r_i = 0.7 mm and f = 40 kHz, or 110 kHz, or 200 kHz.

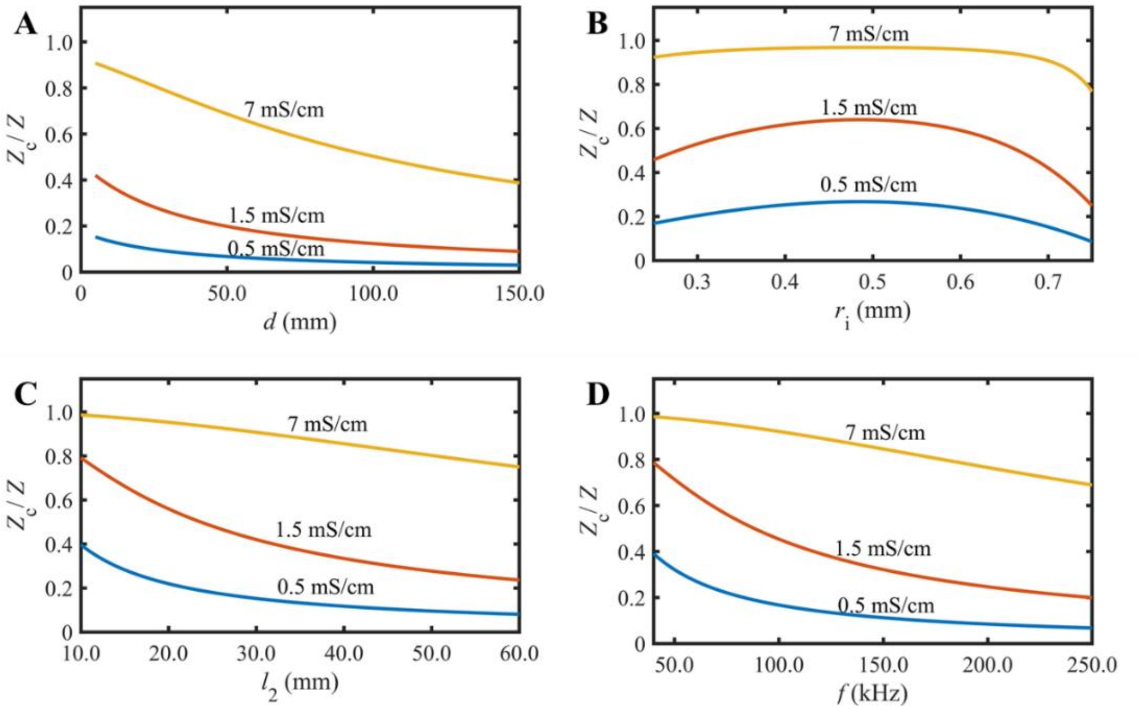

Figure S4. Characteristic curves of Z_c/Z and d, r_i, l_2, f with different conductivities. Digital computation parameters: $\varepsilon_0 = 8.8542\times10^{-12}$ F/m, ε_r = 3.2, R_f = 1 MΩ, C_f = 5 pF, V_{pp} = 20 V, r_o = 0.8 mm, l_1 = 30 mm and σ = 0.5 mS/cm, or 1.5 mS/cm, or 7 mS/cm. (**A**) d is from 5 mm to 150 mm, l_2 = 30 mm, r_i = 0.7 mm, f = 110 kHz. (**B**) d = 5 mm, l_2 = 30 mm, r_i is from 0.25 mm to 0.75 mm, f = 110 kHz. (**C**) d = 5 mm, l_2 is from 10 mm to 60 mm, r_i = 0.7 mm, f = 110 kHz. (**D**) d = 5 mm, l_2 = 30 mm, r_i = 0.7 mm, f is adjusted from 40 kHz to 250 KHz.

Table S1. Comparisons of Z_c/Z in different gears (σ = 7 mS/cm).

	M-C^{4}D (r_i = 0.375 mm)	M-C^{4}D (r_i = 0.5 mm)	M-C^{4}D (r_i = 0.7 mm)
Z_c/Z of gear 1	0.93	0.94	0.84
Z_c/Z of gear 2	0.70	0.74	0.52
Z_c/Z of gear 3	0.47	0.50	0.31

Table S2. Comparisons of relative sensitivity (RS) in different gears.

	M-C^{4}D (r_i = 0.375 mm)	M-C^{4}D (r_i = 0.5 mm)	M-C^{4}D (r_i = 0.7 mm)
RS of gear 1 (%)	0.95	0.89	0.86
RS of gear 2 (%)	0.56	0.39	0.55
RS of gear 3 (%)	0.72	0.55	0.99

Figure S5. The specifications of ET130 C^4D detector headstage (https://www.edaq.com/ET130).

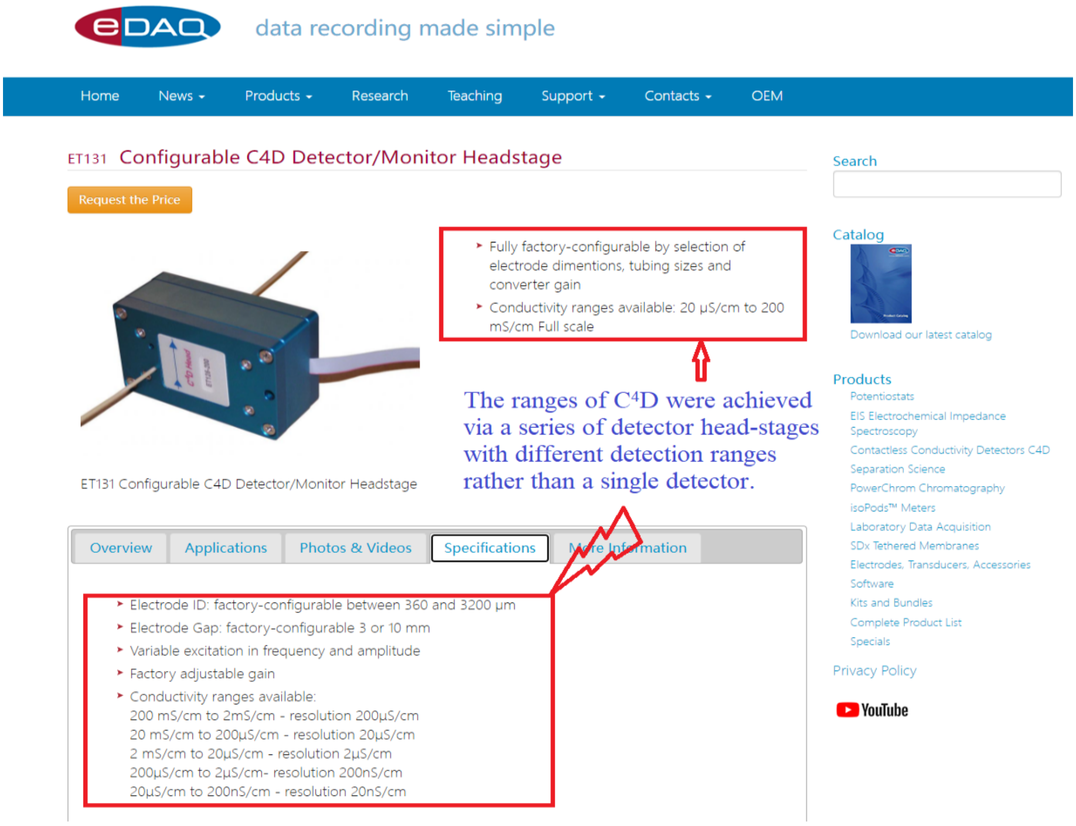

Figure S6. The specifications of ET131 C^4D detector headstage (https://www.edaq.com/ET131).

S4. The detection ranges of DDS and C^4D detectors.

Figure S5 was the web screenshot of the specifications of ET130 C^4D detector headstage. **Figure S6** was the web screenshot of the specifications of ET131 C^4D detector headstage. **Figure S7** was the web screenshot of the specifications of DDS-307.The ranges of DDS and C^4D were achieved via a series of detector head-stages with different detection ranges, rather than a single detector. Although the single detector head-stage of DDS currently used could achieve the range of 0.015-20 mS/cm obtained herein, the single detector head-stage of C^4D could not achieve this range.

Figure S7. The specifications of DDS-307. (**A**) https://www.inesarex.com/conductivity-meter/57581897.html#module_attr. (**B**) https://www.inesarex.com/conductivity-electrode/57588299.html

S5. Conductivity test of KCl solutions at different temperatures.

Temperature effect is a common problem of C^4D sensor because conductivities is temperature-dependent. When the temperature changes, the conductivity of the solution also changes. Figure S8 showed the conductivity curves of KCl solutions at different temperatures measured via both the online contactless M-C4D sensor and the offline contact DDS meter.

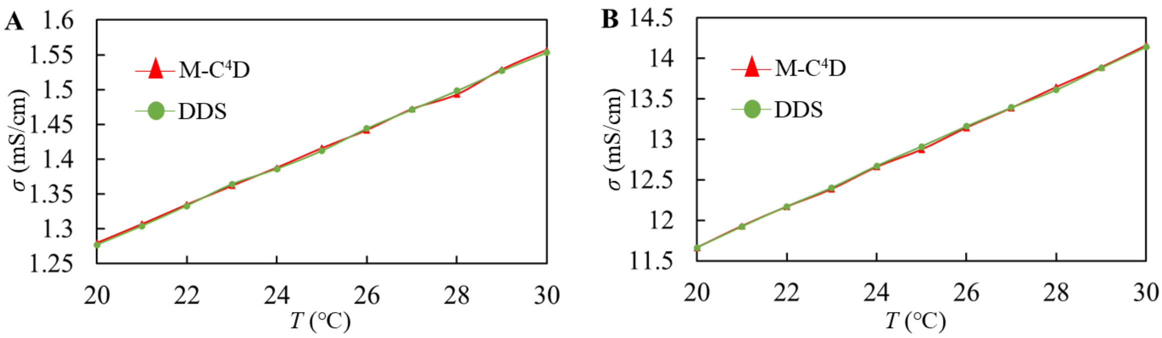

Figure S8. Conductivity curves of KCl solutions at different temperatures measured via both the online contactless M-C^4D sensor and the offline contact DDS meter. 10 mM KCl (**A**) and 100 mM KCl (**B**).